Electronic Supplementary Material (ESI) for Physical Chemistry Chemical Physics.

Origin of hydroxyl pair formation on reduced anatase TiO_2(101)

Supporting Information

Kræn C. Adamsen,[1] Nikolay G. Petrik,[2*] Wilke Dononelli,[3,4] Greg A. Kimmel,[2] Tao Xu,[1] Zheshen Li,[3] Lutz Lammich,[1,3] Bjørk Hammer,[3] Jeppe V. Lauritsen,[1] and Stefan Wendt[1*]

[1]*Interdisciplinary Nanoscience Center (iNANO), Aarhus University, DK-8000 Aarhus C, Denmark.*

[2]*Physical Sciences Division, Pacific Northwest National Laboratory, Richland, Washington 99352, USA.*

[3]*Department of Physics and Astronomy, Aarhus University, DK-8000 Aarhus C, Denmark.*

[4]*MAPEX Center for Materials and Processes, Bremen Center for Computational Materials Science and Hybrid Materials Interfaces Group, Bremen University, 28359 Bremen, Germany*

[*]Corresponding authors: swendt@inano.au.dk; nikolay.petrik@gmail.com

1 Experimental details of the IRRAS, TPD and ESD experiments

The IRRAS, TPD and ESD experiments were performed at PNNL in Richland, USA. An ultrahigh vacuum (UHV) system was used that is similar to that described previously.[1, 2] The system with a base pressure of ~1 × 10^{-10} Torr was equipped with a molecular beam source, a closed-cycle helium cryostat for sample cooling, a low-energy electron gun (Kimball Physics, model ELG-2), quadrupole mass spectrometer (Extrel, model EXM720), and a Fourier-transform infrared (FTIR) spectrometer (Bruker, Vertex 80) for IRRAS measurements performed in external reflection mode.

Thin water films were deposited with a molecular beam doser (flux ~2 × 10^{14} molecules / cm^2 s) at normal incidence to the surface (typically at 120 K sample temperature). The molecular beam doser consists of 3 differentially pumped stages separated by apertures. The beam was turned on and off using micro-dispensing solenoid valves (The Lee Co., No. INKX0514900A) with ~1 ms time resolution. Thus, despite the relatively high water flux, accurate and reproducible water doses were obtained. The molecular beam produced a film centred on the substrate having a diameter of 7.0 mm for the umbra and 7.6 mm for the penumbra. As can be seen in Fig. S1c, the beam spot

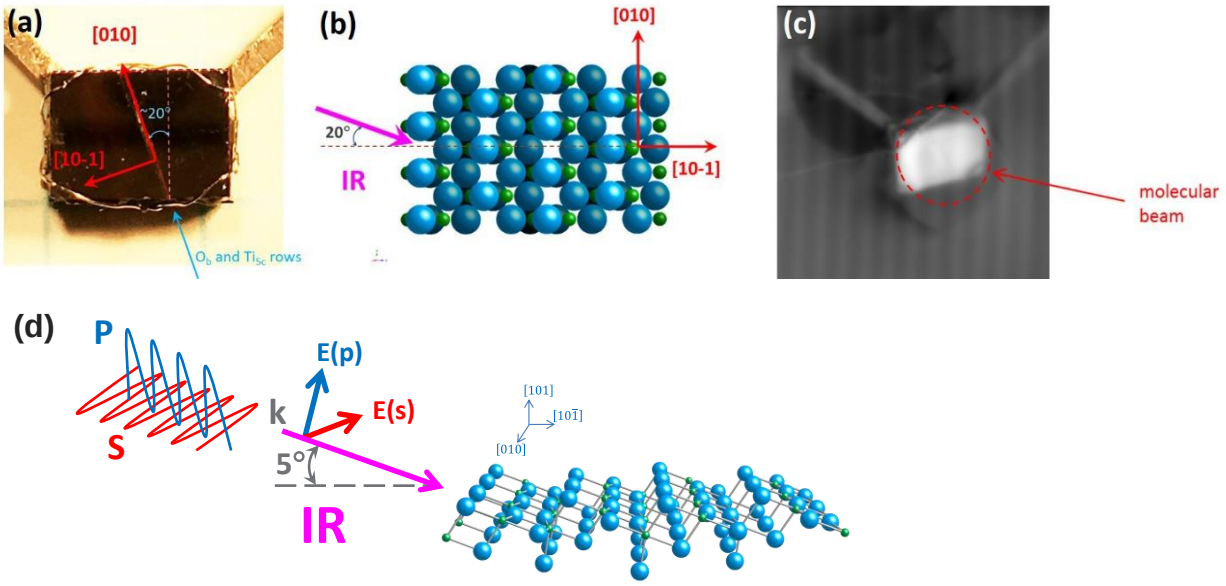

Fig. S1 (a) a-TiO_2(101) sample with size (7 × 5 × 2 mm^3) mounted on a tantalum plate holder using Aremco cement and thin tantalum wires at the corners. (b) The IR beam comes normally to the shorter (5 mm) side of the sample at 20° to the $[10\bar{1}]$ azimuth at glancing angle to the (101) surface (5°). (c) Secondary electron image of the sample with a dosed H_2O film (white spot). The molecular beam ∅ 7.3 mm (umbra), centered on the sample and larger than the sample. (d) Schematic of the IRRAS geometry on TiO_2(101). For s-polarized light, the electric field, E(s), is parallel to the (101) surface and perpendicular to the IR beam direction shown in (b). For the geometry shown, s-polarized spectra are sensitive to vibrations with a transition dipole moment that has a component parallel to the surface and perpendicular to the direction of the IR beam. For p-polarized light, the electric field, E(p), has components normal and parallel to the surface. Thus p-polarized spectra are sensitive to transition dipole moments perpendicular to the (101) surface and parallel to the surface in the direction of the IR beam.

was in the vertical dimension slightly larger than the anatase sample ($7 \times 5 \times 2$ mm^3). One monolayer (ML) coverage of water is defined as the desorption yield from 5f–Ti sites in the TPD spectra (5.2×10^{14} molecules/cm^2) of a rutile TiO_2(110) single crystal that was used for calibration of the water beam flux. Rutile TiO_2(110) single crystals are better suited for the calibration of the water flux because the 1st ML of water is well-resolved in the TPD spectra (in case of anatase TiO_2(101), the 1st ML and the 2nd ML are not well resolved in water TPD spectra, see Fig. S3).

The used natural mineral anatase crystal with a miscut angle smaller than 0.3º was purchased from SurfaceNet. The sample was mounted on a tantalum plate using high-temperature conducting cement (Aremco 865) and thin tantalum wires (see Fig. S1a). The anatase sample was heated by resistively heating the base plate. The temperature was monitored by a K-type thermocouple spot-welded to the base plate. For the relatively thick (2 mm) natural mineral anatase crystals, we expect a significant thermal gradient between the base plate and the external surface of the anatase sample during the relative fast (2 K / s) temperature ramp. As a result, the apparent temperatures in our TPD spectra are higher than the previously reported for thinner crystals and slower ramps. We have performed surface temperature calibration at various heating rates by analyzing zero-order TPD spectra of multilayer coverages of H_2O and CO_2 ices. For multilayers, the leading edges of the multilayer desorption features are independent of the ramp rate and can be compared with the standard vapor pressure data versus temperature.[3] At 2 K / s, the difference between the temperatures of the TiO_2 front face and the back-plate can be as high as ~100 K. However, for isothermal measurements the temperature gradient across the sample is minimal. The sample was cleaned by repeated cycles of sputtering with 2 keV Ne^+ followed by 4 minutes annealing at 720 K under O_2 beam, and vacuum-annealing at 950 K,[4] after which a sharp (1 × 1) LEED pattern was observed.

For sample irradiation, an electron beam was directed at 40° with respect to the sample normal. The incident energy of the electrons, E_i, used to irradiate the films was typically 500 eV, and the instantaneous current densities were ~3.3×10^{15} cm^{-2} s^{-1} as measured with a Faraday cup. The electron beam was smaller than the molecular beam spot size on the sample (~1.5 mm and 7.0 mm, respectively). To produce a uniform electron fluence across the films, the electron beam was rastered over the area slightly larger than the water spot, delivering 3.5×10^{13} electrons / cm^2 for each 0.4 s scan. The ESD signals are an average of all data points in each scan. Throughout the irradiation, the temperature was 100 K.

In the IRRAS experiments, the s- or p-polarized infrared (IR) light was incident on the a-TiO_2(101) single crystal at 20° to the $[10\bar{1}]$ azimuth and grazing incidence (~85° with respect to the surface normal) and detected in the specular direction (see Fig. S1b). For s-polarized light, the electric field vector was parallel to surface and therefore, those spectra were sensitive to vibrations that have transition dipole moments parallel to the surface. We note that on a dielectric substrate for s-polarized light, the absorbance, $A = \log_{10}(R_0/R)$, is always negative due to optical effects[5, 6] (R and R_0 are the reflected light intensities (or reflectivities) of the clean and the water-covered surfaces). For p-polarized light, the electric field vector has components perpendicular and parallel to the surface. For the geometry used in the IRRAS experiments, modes that are perpendicular to the surface showed up as negative absorbance ("emission") peaks, while modes that are parallel to the

surface showed up as positive peaks.[5, 7] Each individual IRRAS experiment includes 2000 interferometer scans from the reference surface (clean a-TiO_2(101)) and 2000 interferometer scans from the surface with the water layer. All the IRRAS measurements were collected at ~30 K. The presented IRRAS spectra are the average of anywhere from 8 to 50 individual experiments (more individual experiments for low coverages). The resolution was set to 4 cm^{-1}.

2 Density of OH_t / OH_b–pairs on a-TiO_2(101)–OH observed by STM

Fig. S2 summarizes our STM studies addressing a-TiO_2(101)–OH prepared via relatively high H_2O exposures at RT. Even after a H_2O exposure of 3000 L the density of OH_t / OH_b–pairs might not have reached saturation.

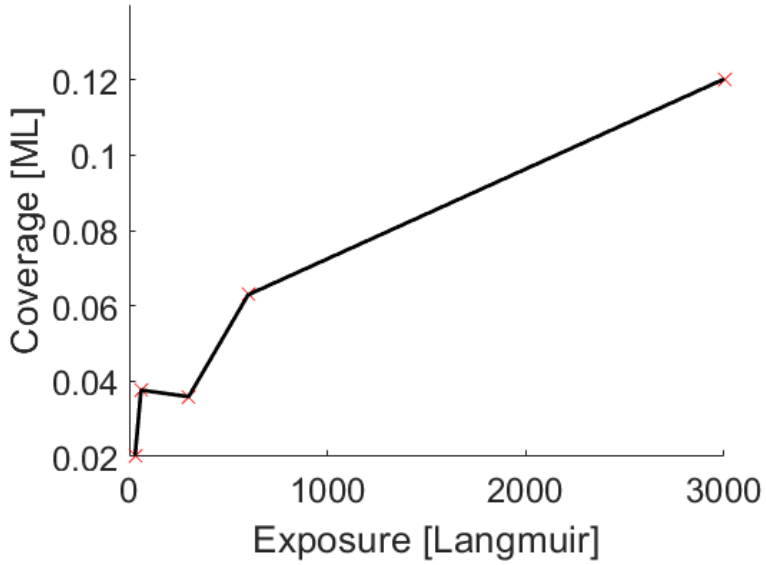

Fig. S2 Density of OH_t / OH_b–pair features as function of the water exposure at RT. Several high-resolution STM images of five STM experiments were analysed to extract the density of OH_t / OH_b–pair features in the experiments.

3 TPD spectra of D_2O / a-TiO_2(101)

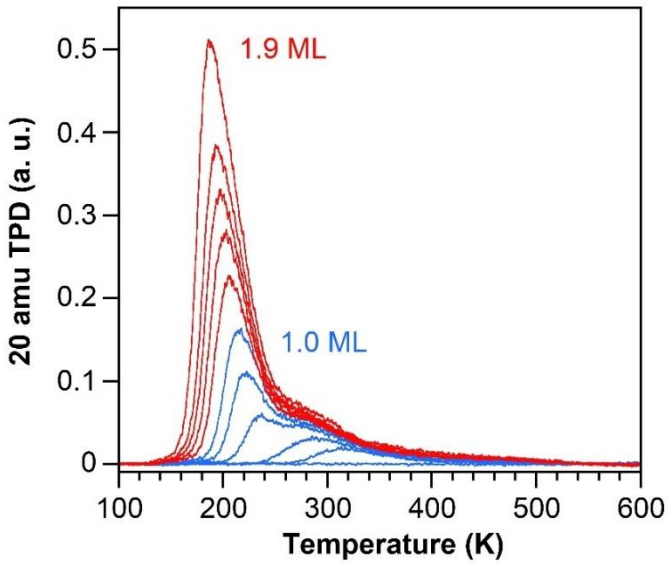

Fig. S3 TPD filling curve: D_2O-TPD spectra for coverages up to 1.9 ML. D_2O was dosed onto a-TiO_2(101) at 100 K. The TPD heating ramp was 2 K/s.

4 D_2O / a-TiO_2(101) - TPD spectra acquired following the ice-treatment

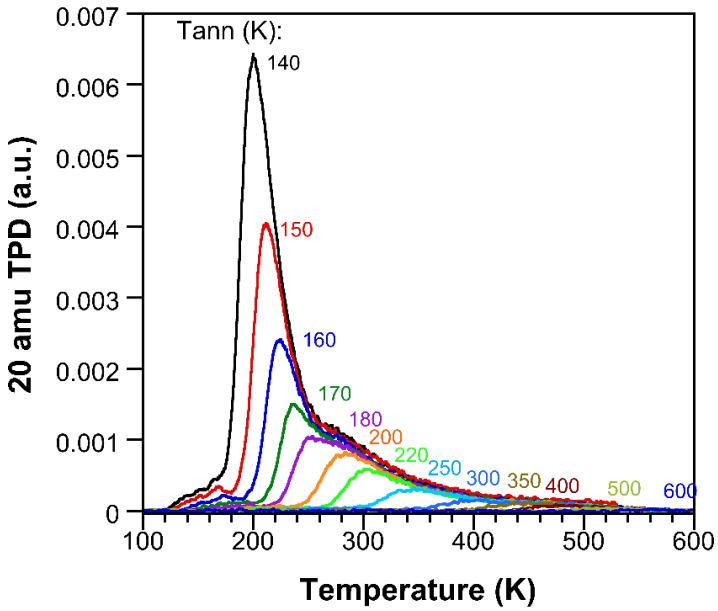

Fig. S4 TPD spectra acquired after 6 ML D_2O exposure at 100 K, followed by annealing at the specified temperatures, T_{ann}, for 600 s. The TPD heating ramp was 2 K/s.

The TPD spectra presented in Fig. S4 show how much water and / or hydroxyl groups were left on the a-TiO_2(101) surface after applying the ice-treatment. In each experiment, the a-TiO_2(101) surface was exposed to 6 ML D_2O at 100 K, followed by annealing at the specified temperatures for 600 s. Of course, how much water desorbs depends on the annealing temperature, T_{ann}. For example, for T_{ann} = 200 K (dark yellow trace) the amount of desorbing D_2O corresponds to ~0.5 ML, and for T_{ann} = 220 K (light green trace) ~0.37 ML D_2O desorbed. Accordingly, when applying the ice-treatment, most of the adsorbed water ice desorbs upon mild vacuum-annealing.

5 IRRAS spectra of annealed D_2O / a-TiO_2(101) samples for s- and p-polarized light

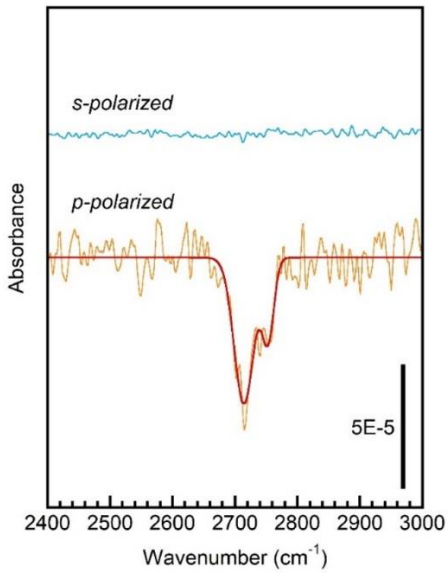

Fig. S5 IRRAS spectra acquired after 6 ML D_2O exposure at 120 K, followed by annealing at 220 K (ice-treatment). Top spectrum: s-polarized light. Bottom spectrum: p-polarized light.

Fig. S5 shows that the ice-treatment led to surface species on a-TiO_2(101) that can exclusively be probed with p-polarized light. Using s-polarized light, we obtained a featureless spectrum (there is only noise).

6 D_2O / a-TiO_2(101) studied by electron-stimulated desorption (ESD)

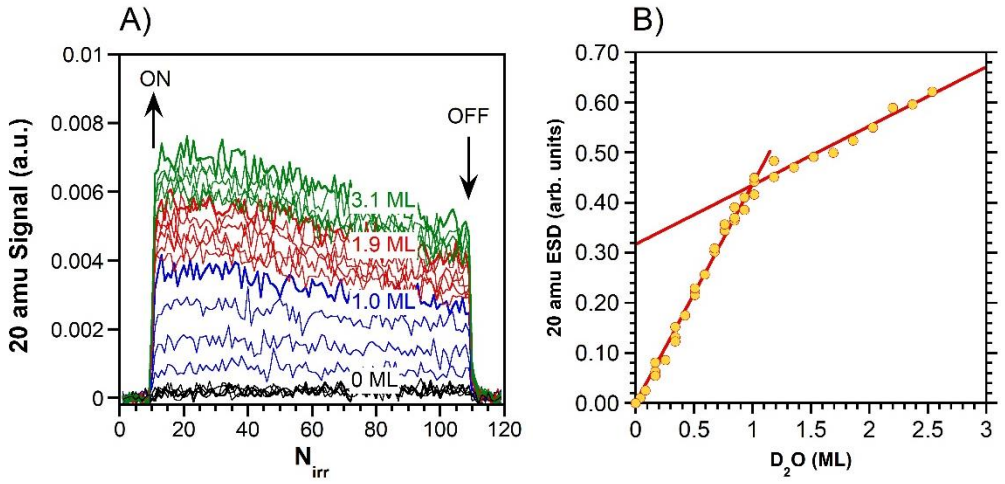

Fig. S6 (a) 20 amu ESD signals versus the irradiation fluence (i.e. number of the irradiation scans, N_{irr}) for different D_2O coverages on a-TiO_2(101). D_2O was dosed at 120 K. The sample was irradiated with 500 eV electrons at 100 K. Instantaneous current densities were ~3.3×10^{15} $cm^{-2}s^{-1}$. The electron beam was rastered over an area slightly larger than the water spot. Arrows mark the times when the electron beam was turned ON and OFF. With no D_2O dosed on the sample, a small (background) signal at 20 amu, which did not change appreciable over the course of the experiments, was observed during electron irradiation (black lines for 0 ML). These signals were subtracted before integration. (b) Integrated initial ESD signals of the first 100 irradiation cycles as function of the D_2O coverage.

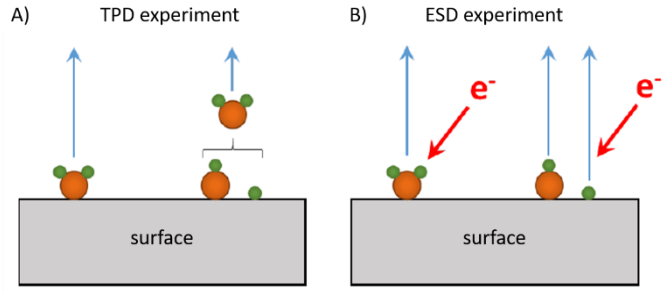

Fig. S7 Comparison of TPD (a) and ESD (b) experiments addressing water / a-TiO_2(101). The TPD signal is associated with both, molecular water and dissociative water, because the dissociation products recombine during temperature ramping. In ESD, the temperature was kept constant during e^- impingement (here at 100 K). This means that exclusively molecular water was probed.

In addition to TPD, we have used electron stimulated desorption (ESD) to study the water / a-TiO_2(101) system (see Fig. S6 as an example). Such ESD studies are interesting, particularly because the combination of TPD and ESD makes it possible to distinguish between molecular and dissociated water species. This was shown previously for water adsorbed on rutile TiO_2(110).[1, 8, 9]

The basic concept is that ESD probes exclusively molecular water (here D_2O, 20 amu), whereas TPD probes both – molecular *and* dissociated water. This important difference is highlighted in the schematic shown in Fig. S7. The reason behind this difference is that the water dissociation products recombine during ramping the temperature within the TPD experiment. In contrast, ESD is typically conducted at low temperatures (here at 100 K), and recombination of the dissociation product is not stimulated upon irradiation with electrons.

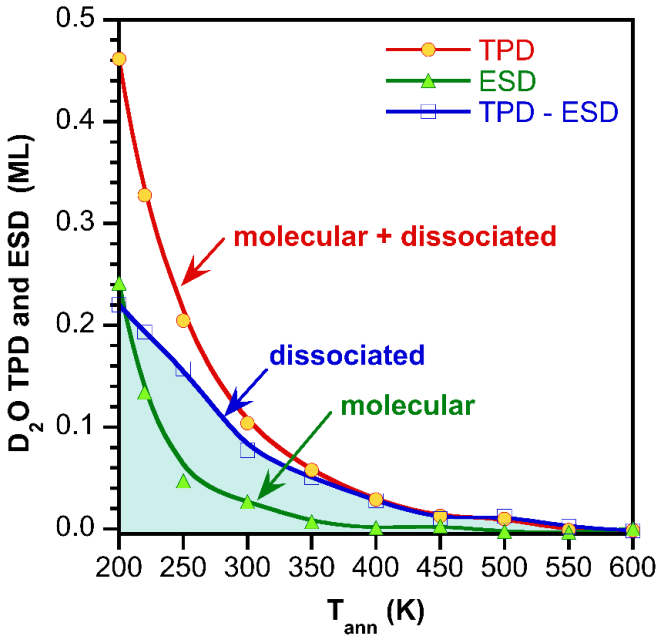

.

Fig. S8 Water coverages as function of T_{ann} after applying the ice-treatment (6 ML D_2O at 100 K followed by annealing at T_{ann} for 600 s). Coverages (20 amu) were estimated by TPD (see Fig. S4) and ESD. The coverages extracted from the TPD traces (red curve) include both molecular and dissociated water species. By ESD (green curve), solely molecular water is probed. The difference between the TPD and ESD coverages (blue curve) is a measure of the "coverage of dissociated water". For the calibration of the D_2O coverages we used the ESD data presented in Fig. S6.

Fig. S8 summarizes our TPD and ESD results obtained after applying the ice-treatment. In each experiment, the a-TiO_2(101) surface was exposed to 6 ML D_2O at 100 K, followed by annealing at the specified temperatures for 600 s. The integrated areas of the 20 amu TPD and ESD traces are shown as function of T_{ann}. Integrated areas labeled "TPD" (red curve) correspond to the TPD traces presented in Fig. S4. The green curve shows the integrated areas deduced from corresponding ESD experiments (data not shown). In addition, we subtracted the green curve (ESD) from the red curve (TPD). The result is the curve shown in blue, which should indicate the coverage of dissociated water species (i.e. hydroxyl groups) on a-TiO_2(101) after applying the ice-treatment. It can be seen that for T_{ann} = 200 K, in total, ~0.5 ML water remained on the surface, and ~50% of it was molecular and ~50 % dissociated. For annealing temperatures higher than 200 K, more water was dissociated, and for T_{ann} higher than ~350 K all the adsorbed water was

dissociated. After annealing at 350 K, only ~0.05 ML water remained on the surface. The data presented in Fig. S8 are in line with the IRRAS and UPS data presented in Fig. 3 of the main article. It is likely that the long tails in the water-TPD spectra arise from dissociated water. That is, hydroxyl groups first need to recombine during ramping the temperature before they desorb as water molecules from the a-TiO_2(101) surface.

7 Water and hydroxyl structures on a-TiO_2(101) modeled by DFT and DFT + U

In order to better interpret the experimental observations, we performed DFT calculations. We compared different adsorption modes of water, including molecular adsorption of a water molecule on 5f–Ti, a dissociated terminal and bridging hydroxyl pair (OD_t / OD_b–pair) where one of the hydrogen atoms is transferred to a neighboring bridging O atom (O_b), and a pair of two bridging hydroxyls. Stoichiometric and reduced a-TiO_2(101) slabs were used. In what follows, stoichiometric slabs are denoted as "sa-TiO_2" and reduced ones as "ra-TiO_2". Here, ra-TiO_2 slabs were created by the introduction of one O_{vac}. As described below, we tested several positions of the O_{vac}.

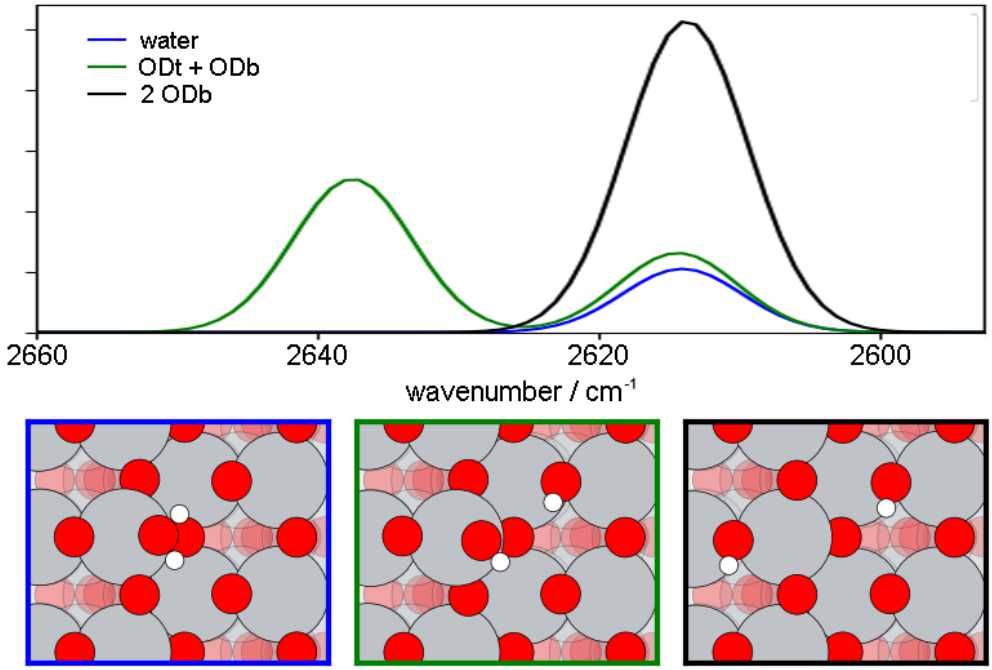

Fig. S9 IRRAS spectra and corresponding structures modeled by DFT, considering the antisymmetric stretching vibration of water (D_2O) and OD stretching vibrations of the OD_t and OD_b hydroxyl groups. Deuterated species were used. We used plain PBE and an sa-TiO_2 slab to model these IRRAS spectra. The calculated vibrational energies are given in Table S1, both for plain PBE and PBE + U. The used Python script for plotting the IR spectra is provided in section 10.

Table S1 Computed vibrational energies (in cm^{-1}) of the antisymmetric OD stretching of a water molecule and OD groups corresponding to the configurations shown in Fig. S9.

Configuration (see Fig. S9)	PBE	PBE + U
D_2O	2614.0	2639.2
OD_t / OD_b–pair	2614.3 (b) 2637.5 (t)	2630.1 (b) 2681.3 (t)
2 × OD_b	2611.7 2614.1	2621.8 2623.3

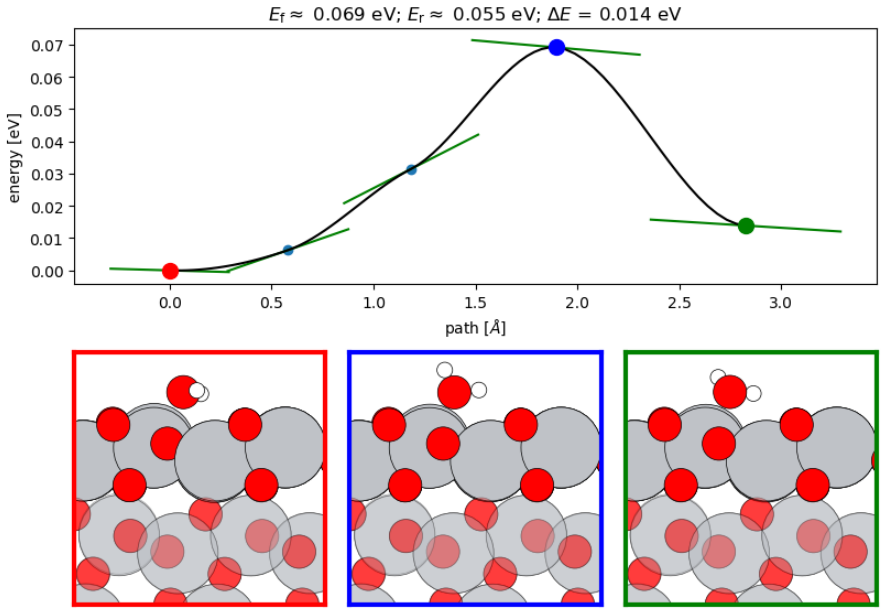

Fig. S10 Rotation barrier between two nearly degenerated states of adsorbed H_2O (ΔE = 14 meV) calculated with plain DFT. Using DFT + U, the barrier is almost identical (E_f = 0.072 eV), whereas the rotated state is slightly less stable using DFT + U (ΔE = 64 meV). Dots represent calculated NEB images; black line is the interpolated DFT energy between images, green lines present force components of images. E_f is the forward barrier, E_r is the reverse activation barrier.

Fig. S9 shows the computed most favorable structures together with the corresponding simulated IRRAS spectra for sa-TiO_2(101). For better comparison to the experimental IRRAS data, we considered D_2O on 5f–Ti, an OD_t / OD_b–pair, and an OD_b–pair (2 × OD_b). To calculate the vibrational modes of the three considered structures, we used the harmonic approximation and finite differences. Because we are mainly interested in the vibration of the molecule, we used the partial Hessian approach. Thus, only vibrational motion of the adsorbed species were allowed.

In its most stable configuration, the water molecule is aligned parallel to the surface (see Fig. S9 and S10). Accordingly, water is expected to be IR-inactive in this configuration. However, the water molecule can easily rotate to an only 14 meV less stable, rotated configuration (see Fig. S10). Such rotated water species are IR active with p-polarized light. As can be seen in Fig. S10, the barrier between the most stable and the rotated configuration is with 69 meV negligible.

Compared to the experimentally observed vibrational energies, the computed vibrational energies (Table S1) are shifted due to the used functional, which is a common, well-known issue. Importantly, the differences of the theoretically deduced vibrational energies are in good agreement with the differences of the experimental vibrational energies. We trust the vibrational energies calculated with plane PBE (without the Hubbart U correction) more than those computed with the Hubbart U correction, as this correction seems to introduce unphysical variations to the vibrational energies, as discussed by German *et al.*[10] The observed trends support the view that the three computed structural motifs shown in Fig. S9 indeed correspond to the peaks found in the IRRAS experiments presented in the main article.

8 DFT calculations addressing the influence of O_{vac}'s in the near-surface region

Using an sa-TiO_2 slab, the water molecule is by 0.32 eV (0.29 with Hubbart U correction) more stable than an OH_t / OH_b–pair. However, if an O_{vac} is introduced into the slab, both types of hydroxyl pairs are more stable than a water molecule (see Table S2). If the O_{vac} is located directly at the surface (see Fig. S11), the 2 × OH_b configuration is most stable. Although the absolute energies computed with plain PBE and PBE+U differ, the general trend is similar. The 2 × OH_b configuration is most stable. Similarly, for surface O_{vac}'s, the OH_t / OH_b–pair is more stable than adsorbed water. An O_{vac} in the subsurface at deeper positions than considered here, or in the bulk, will lead to a change of the energetic order such that molecular water becomes more stable than the OH_t / OH_b–pair. If there is no surface O_{vac}, the 2 × OH_b configuration cannot be formed.

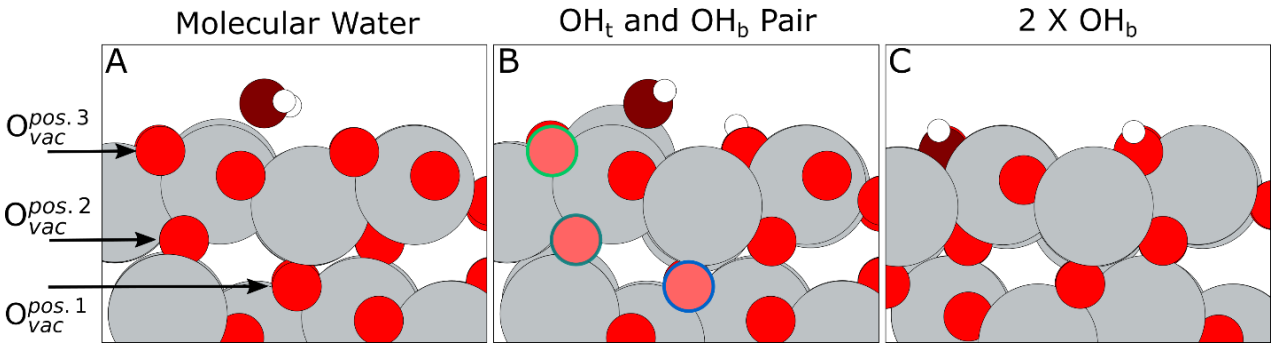

Fig. S11 Most stable configurations (PBE functional) of a) molecular water, b) an OH_t / OH_b–pair, and c) a 2 × OH_b configuration on ra-TiO_2(101). In a), the three considered O_{vac} positions are indicated. Corresponding adsorption energies are given in Table S2.

Table S2 (same as Table 1 in the main article) Relative adsorption energies (in eV) of the considered H_2O and hydroxyl structures on ra-TiO_2(101) and sa-TiO_2(101) computed with PBE and PBE+U. Minus signs indicate that the hydroxyl structures are more stable than molecular water. For the O_{vac} positions, see Fig. S11 and/or Fig. 5.

ra-TiO_2(101)	PBE	PBE+U
O_{vac} at position 1: molecular water on 5f–Ti *vs.* OH_t / OH_b	–0.15	–0.11
O_{vac} at position 2: molecular water on 5f–Ti *vs.* OH_t / OH_b	–0.16	–0.05
O_{vac} at position 3: molecular water on 5f–Ti *vs.* OH_t / OH_b	–0.35	–0.20
O_{vac} at position 3: molecular water on 5f–Ti *vs.* 2 × OH_b	–0.42	–0.62
O_{vac} at position 3: molecular water in O_{vac} *vs.* 2 × OH_b	–0.59	–0.58
sa-TiO_2(101)		
no O_{vac}: molecular water on 5f–Ti *vs.* OH_t / OH_b	+0.32	+0.29

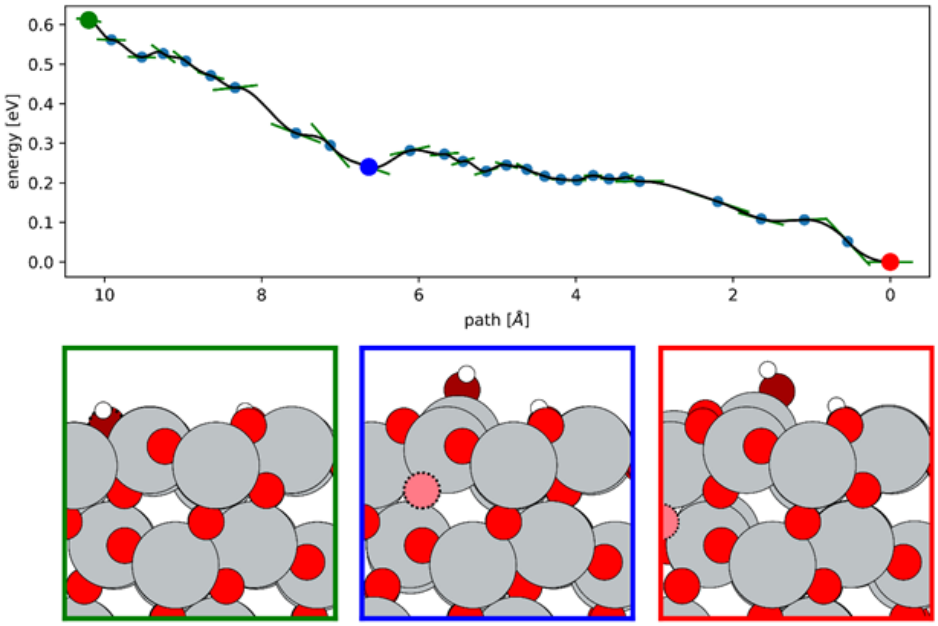

Fig. S12 Diffusion path of the O_{vac}, migrating from position 1 to position 3 (surface) going from the red frame to the blue and then the green frame. In this path, the adsorbed OH_t is converted to an OH_b, thereby filling the O_{vac}. In the considered ra-TiO_2 slab, this happens without significant barriers and is driven by an energy gain of ~0.6 eV. The NEB pathway was calculated using the PBE functional. Dots represent calculated NEB images; black line is the interpolated DFT energy between images, green lines present force components of images. E_f is the forward barrier, E_r is the reverse activation barrier.

In order to understand the possibility of O_{vac} diffusion in a-TiO_2, we performed NEB calculations with a total number of 26 images between the initial and final state, see Fig. S12. In agreement with a previous DFT study,[11] we found that the O_{vac}'s migrate through the upper TiO_2 tri-layer without any significant barrier, eventually forming the 2 × OH_b configuration. These barriers, and also the barriers addressing OH_t / OH_b–pair formation from molecular water (see Fig. 5 of the main article), were calculated without the Hubbard correction.

9 Removal of the hydroxyl pairs from the a-TiO_2(101) surface

Having established that OH_t / OH_b (or OD_t / OD_b)–pairs form on the a-TiO_2(101) surface, we discuss how such hydroxyl pairs can be removed upon heating and annealing of the sample. On the basis of the IRRAS data shown in Fig. 3 of the main article, we conclude that most OD_t / OD_b–pairs simply recombine when the temperature is ramped up. This scenario is consistent with the fact that the IRRAS peaks within the doublet disappear almost simultaneously upon annealing. However, a narrow $O–D^{D2O}$ + OD_b peak was still detectable even after annealing at 500 K, whereas the OD_t peak disappeared upon annealing at 450–500 K (Fig. 3b). Considering our DFT results (see Fig. 5 and S11 and Table S2), it is likely that, at sufficiently high annealing temperatures, some OD_t / OD_b–pairs have transformed into 2 × OD_b configurations. If the temperature increases further, the remaining OH_b (OD_b) species may disappear from the a-TiO_2(101) surface through H (or D) migration into the bulk.[12-15] Notice that we did not find signs for H_2 (or D_2) desorption, as observed for a-TiO_2(101) surfaces that were irradiated with electrons prior to water exposure.[12] Furthermore, notice that there is no indication in our (see Fig. S2 and S3) and previous TPD data[12, 16] that remaining OH_b species recombine with surface O atoms and then desorb as water.

10 Python script for IR spectra simulation

```
############ Begin Python script for plotting IR spectra for list of given
wavenumbers and intensities ###################
import numpy as np

"""
This python script has been adapted from the atomistic simulation environment ASE
but reduced in its complexity
It should run under any Python3 version and only needs the numpy package

If you are using it to plot IR spectra, please cite:
        Ask Hjorth Larsen et al 2017 J. Phys.: Condens. Matter 29 273002
        DOI 10.1088/1361-648X/aa680e

In addition, you are very welcome to cite this underlying work:
        Krean Adamsen et al, Origin of Hydroxyl Pair Formation on Reduced
        Anatase TiO2(101), 2023, PCCP
```

```
The last three lines of this script have to be adjusted to plot new spectra
"""

def fold(frequencies, intensities,
        start=800.0, end=4000.0, npts=None, width=4.0,
        type='Gaussian', normalize=False):
        """Fold frequencies and intensities within the given range
        and folding method (Gaussian/Lorentzian).
        The energy unit is cm^-1.
        normalize=True ensures the integral over the peaks to give the
        intensity.
        """

        lctype = type.lower()
        assert lctype in ['gaussian', 'lorentzian']
        if not npts:
            npts = int((end - start) / width * 10 + 1)
        prefactor = 1
        if lctype == 'lorentzian':
            intensities = intensities * width * np.pi / 2.
            if normalize:
                prefactor = 2. / width / np.pi
        else:
            sigma = width / 2. / np.sqrt(2. * np.log(2.))
            if normalize:
                prefactor = 1. / sigma / np.sqrt(2 * np.pi)

        # Make array with spectrum data
        spectrum = np.empty(npts)
        energies = np.linspace(start, end, npts)
        for i, energy in enumerate(energies):
            energies[i] = energy
            if lctype == 'lorentzian':
                spectrum[i] = (intensities * 0.5 * width / np.pi /
                               ((frequencies - energy)**2 +
                                0.25 * width**2)).sum()
            else:
                spectrum[i] = (intensities *
                               np.exp(-(frequencies - energy)**2 /
                                      2. / sigma**2)).sum()
        return [energies, prefactor * spectrum]


def write_spectra(frequencies, intensities, out='ir-spectra.dat', start=800,
        end=4000, npts=None, width=10, type='Gaussian', normalize=False):
```

```
        """Write out infrared spectrum to file.

        First column is the wavenumber in cm^-1, the second column the
        absolute infrared intensities, and
        the third column the absorbance scaled so that data runs
        from 1 to 0. Start and end
        point, and width of the Gaussian/Lorentzian should be given
        in cm^-1."""

        energies, spectrum =fold(frequencies, intensities,
                         start, end, npts, width, type, normalize)

        # Write out spectrum in file. First column is absolute intensities.
        # Second column is absorbance scaled so that data runs from 1 to 0
        spectrum2 = 1. - spectrum / spectrum.max()
        outdata = np.empty([len(energies), 3])
        outdata.T[0] = energies
        outdata.T[1] = spectrum
        outdata.T[2] = spectrum2
        with open(out, 'w') as fd:
            fd.write('# %s folded, width=%g cm^-1\n' % (type.title(), width))
            iu, iu_string = 1.0, '(D/Å)^2 amu^-1'
            if normalize:
                iu_string = 'cm ' + iu_string
            fd.write('# [cm^-1] %14s\n' % ('[' + iu_string + ']'))
            for row in outdata:
                fd.write('%.3f  %15.5e  %15.5e \n' %
                         (row[0], iu * row[1], row[2]))


##########################################Main
code################################################
##List of frequencies and list of corresponding intensities
example_freq =   [1158.0, 2519.7, 2614.0]
example_intens = [0.2463, 0.2779, 0.5232]

#Write the spectrum by placing either Gaussian or Lorentzian Function with given
width (e.g. 10 cm^-1) at position of given frequencies
write_spectra(frequencies= example_freq, intensities=example_intens,out='ir-
spectra.dat',start=300,end=4000,width=10,type='Gaussian')


############ End Python script for plotting IR spectra for list of given
wavenumbers and intensities ##################
```

References of the Supporting Information

1 C. D. Lane, N. G. Petrik, T. M. Orlando and G. A. Kimmel, *J. Phys. Chem. C* 2007, **111**, 16319–16329.

2 N. G. Petrik and G. A. Kimmel, *J. Phys. Chem. C* 2009, **113**, 4451–4460.

3 H. Schlichting and D. Menzel, *Rev. Sci. Instrum.* 1993, **64**, 2013–2022.

4 M. Setvin, B. Daniel, V. Mansfeldova, L. Kavan, P. Scheiber, M. Fidler, M. Schmid and U. Diebold, *Surf. Sci.* 2014, **626**, 61–67.

5 Y. J. Chabal, *Surf. Sci. Rep.* 1988, **8**, 211–357.

6 W. N. Hansen, *J. Opt. Soc. Am.* 1968, **58**, 380.

7 G. A. Kimmel, M. Baer, N. G. Petrik, J. VandeVondele, R. Rousseau and C. J. Mundy, *J. Phys. Chem. Lett.* 2012, **3**, 778–784.

8 N. G. Petrik and G. A. Kimmel, *Phys. Rev. Lett.* 2007, **99**,196103.

9 C. D. Lane, N. G. Petrik, T. M. Orlando and G. A. Kimmel, *J. Chem. Phys.* 2007, **127**, 9.

10 E. German, R. Faccio and A. W. Mombru, *J. Phys. Commun.* 2017, **1**, 10.

11 Y. D. Li and Y. Gao, *Phys. Rev. Lett.* 2014, **112**, 206101.

12 N. A. Deskins, G. A. Kimmel and N. G. Petrik, J. Phys. Chem. Lett. 2020, **11**, 9289–9297.

13 C. H. Sun, Y. Jia, X. H. Yang, H. G. Yang, X. D. Yao, G. Q. Lu, A. Selloni and S. C. Smith, *J. Phys. Chem. C* 2011, **115**, 25590–25594.

14 M. M. Islam, M. Calatayud and G. Pacchioni, *J. Phys. Chem. C* 2011, **115**, 6809–6814.

15 U. Aschauer and A. Selloni, *Phys. Chem. Chem. Phys.* 2012, **14**, 16595–16602.

16 G. S. Herman, Z. Dohnalek, N. Ruzycki and U. Diebold, *J. Phys. Chem. B* 2003, **107**, 2788–2795.